JCIM JOURNAL OF CHEMICAL INFORMATION AND MODELING

pubs.acs.org/jcim Article

Exploring the Spike-hACE 2 Residue−Residue Interaction in Human Coronaviruses SARS-CoV-2, SARS-CoV, and HCoV-NL63

José X. Lima Neto, Davi S. Vieira, Jones de Andrade, and Umberto Laino Fulco*

Cite This: https://doi.org/10.1021/acs.jcim.1c01544 Read Online

ACCESS | Metrics & More | Article Recommendations | Supporting Information

ABSTRACT: Coronaviruses (CoVs) have been responsible for three major outbreaks since the beginning of the 21st century, and the emergence of the recent COVID-19 pandemic has resulted in considerable efforts to design new therapies against coronaviruses. Thus, it is crucial to understand the structural features of their major proteins related to the virus−host interaction. Several studies have shown that from the seven known CoV human pathogens, three of them use the human Angiotensin-Converting Enzyme 2 (hACE-2) to mediate their host's cell entry: SARS-CoV-2, SARS-CoV, and HCoV-NL63. Therefore, we employed quantum biochemistry techniques within the density function theory (DFT) framework and the molecular fragmentation with conjugate caps (MFCC) approach to analyze the interactions between the hACE-2 and the spike protein-RBD of the three CoVs in order to map the hot-spot residues that form the recognition surface for these complexes and define the similarities and differences in the interaction scenario. The total interaction energy evaluated showed a good agreement with the experimental binding affinity order: SARS-2 > SARS > NL63. A detailed investigation revealed the energetically most relevant regions of hACE-2 and the spike protein for each complex, as well as the key residue−residue interactions. Our results provide valuable information to deeply understand the structural behavior and binding site characteristics that could help to develop antiviral therapeutics that inhibit protein−protein interactions between CoVs S protein and hACE-2.

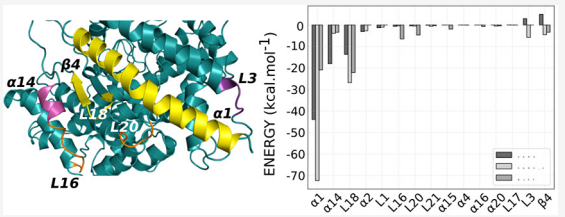

INTRODUCTION

In December 2019, a novel human coronavirus was discovered in the city of Wuhan, China, and designated as Severe Acute Respiratory Syndrome coronavirus 2 (SARS-CoV-2) due to its similarity to the SARS-CoV genome (2002−2003). Commonly referred to as coronavirus disease 19 (COVID-19), this novel coronavirus disease spread to more than 200 countries in a few months. Almost two years after its discovery, ∼247 million infections and over 5 million deaths have been registered all over the world according to the World Health Organization (WHO), and the numbers are increasing daily.[1] Despite all efforts, to date, there is no safe treatment available against CoVs, and the emergence of new variants that can escape from immune surveillance is still a constant risk.

CoVs are enveloped viruses with positive-sense RNA belonging to the *Nidovirales* order, *Coronaviridae* family, and *Coronavirinae* subfamily that is divided into four genera (α, β, γ, and δ types), and can infect a wide range of mammalian and avian species, causing diseases in the liver, as well as in the respiratory, gastrointestinal, renal, and nervous systems.[2,3] Their genome commonly encodes four structural proteins: the spike (S) glycoprotein, the envelope (E) protein, the membrane (M) protein, and the nucleocapsid (N) protein, as well as a series of nonstructural proteins involved in replication and transcription.[4] Among these, the spike glycoprotein is seen as a key target for potential therapies and diagnostics, since it mediates coronavirus recognition and entry into the host cell.[5]

S protein is a trimeric class I fusion protein containing over 1200 amino acids, with each monomer consisting of three segments: ectodomain, transmembrane, and intracellular. In regard to the ectodomain, it is also divided into the S1 receptor-binding subunit and S2 membrane-fusion subunit, with the receptor-binding domain (RBD) and receptor-binding motif (RBM) in S1 being responsible for the recognition of the host's cell receptor.[6,7] From the seven confirmed coronavirus species known as human pathogens, only three of them recognize the same human target to enter into the cell, the Angiotensin-Converting Enzyme 2 (hACE-2; EC: 3.4.17.23): SARS-CoV (β-CoV), SARS-CoV-2 (β-CoV), and HCoV-NL63 (α-CoV), with the last being a prevalent human respiratory pathogen often related to common colds.[8] hACE-2 is a carboxypeptidase widely distributed in the human body that consists of an 805 amino-acid type I transmembrane protein containing, in the extracellular part, a catalytic domain formed by a substrate-binding region, a zinc metallopeptidase domain, and a binding site that CoVs RBM evolved to recognize, the virus-binding motif (VBM).[6,9,10] Thus, inhibit-

Received: December 22, 2021

ing the binding of the RBD-spike protein to VBM-hACE-2 is an attractive strategy for developing antibodies and other potential inhibitors that hinder the viral attachment.[11−13]

Coronaviruses demonstrate a high versatility in viral receptor binding strategies since the S1 amino-acid sequence and structure, as well as the host's receptor target, differ among the CoV's genera.[14] Curiously, only SARS-CoV-2 resulted in a pandemic among the human-infecting CoVs that recognize hACE-2, which led some authors to relate this to differences in the structural conformation of spike protein and a distinct binding interface of SARS-CoV-2 to hACE-2 as compared to other CoVs.[15,16] Recent experimental studies have shown that the SARS-CoV-2 spike has a higher binding affinity toward hACE2 compared to SARS-CoV, while previous data depicted that the HCoV-NL63 receptor-binding affinity is much lower than that of SARS-CoV, which may help explain the differences in these CoVs infectivities and transmissibility.[14,17−20] In this sense, it is vital to deeply investigate the receptor recognition mechanisms of coronaviruses for understanding their pathogenesis and epidemics, as well as for human intervention in coronavirus infections.

In this sense, we investigated the residue−residue interactions in the crystal structure of the hACE2/spike protein complex using *in silico* approaches to deeply understand the mechanism underlying the virus attachment and find the similarities and differences in the interaction pattern of the low pathogenic common cold virus HCoV-NL63 and the high pathogenic SARS viruses (SARS-CoV and SARS-CoV-2). For this purpose, we obtained the three hACE-2/spike protein X-ray structures from the Protein Data Bank (www.rcsb.org/pdb) and employed quantum biochemistry techniques within the density function theory (DFT) framework and the molecular fragmentation with conjugate caps (MFCC) approach to calculate the individual contribution of each amino-acid residue for the protein−protein interface to map the recognition surface for these complexes. These data may shed some light on how different CoVs recognize hACE-2 enzymes and could help the development of novel therapeutic strategies.

MATERIALS AND METHODS

Drug-Receptor Complex Data and Quantum Calculations. We used the X-ray crystallographic data of the human Angiotensin-Converting Enzyme 2 (hACE) solved in complex with the receptor-binding domain (RBD) region of SARS-CoV (PDB ID: 2AJF; 2.90 Å of resolution),[21] SARS-CoV-2 (PDB ID: 6M0J; 2.45 Å of resolution),[22] and HCoV-NL63 (PDB ID: 3KBH; 3.31 Å of resolution).[23] First, we added missing protein amino-acid atoms, and also hydrogen atoms were included according to the results obtained from the PROPKA 3.1 package set up at pH 7.0,[24] as well as for water molecules. Then, protein main-chain heavy atoms are constrained, and all the other atoms are submitted to a classical energy minimization using the Chemistry at Harvard Molecular Mechanics (CHARMm) force field,[25] with the convergence tolerances to 10^{-5} kcal mol^{-1} (total energy variation) and 10^{-2} kcal mol^{-1} Å^{-1} (RMS gradient). Since the PROPKA software is slightly sensitive to the ligand pocket geometry, the steps of hydrogen addition/withdrawal and energy minimization are carried out until no difference is observed in the protonation results.[26]

After the energy minimization step, the three complexes were fragmented following the molecular fractionation with conjugate caps (MFCC; see below) scheme, and the structures generated were submitted to energetic quantum mechanical calculations through the Gaussian (G09) package,[27] within the density functional theory (DFT) formalism. The generalized gradient approximation (GGA) functional B97D[28] was selected to perform the quantum *in silico* simulation, and the 6-311+G(d,p) basis set was chosen to expand the Kohn−Sham orbitals. We have chosen the functional B97D over other methods due to its good performance for noncovalently bound systems. Besides, it was already used in the case of the interaction of nanomaterial−ligand systems,[29] as well as in the evaluation of a large number of data sets proposed by Li et al., in which B97D presents the best performance over some of the hybrid methods applied in their work and is close to functionals using D3 correction, including B3LYP+D3.[30] To improve our results, the effect of the residues' surroundings formed by neighboring atoms (amino acids and water molecules) was included in our calculations through the use of the conductor-like polarizable continuum model (CPCM)[31,32] with the dielectric constant ε_{40}, which represents the influence of the electrostatic environment surrounding the residue−residue complex.[33−35]

Molecular Fractionation with Conjugate Caps. As presented above, we fragmented the protein into amino acids following the MFCC scheme[36,37] adapted by Rodrigues et al. to calculate protein−protein interactions.[38] The MFCC scheme together with DFT calculations have been widely employed to calculate the interaction energies (IEs) in protein−ligand and protein−protein complexes with great success, making the investigation of a large number of amino-acid residues in a protein possible with a small computational cost and high accuracy.[39−43]

In the framework of this approach, for each amino acid of interest of the hACE-2 at position R_i, we mapped its distance to the residues in the spike protein at position R_j and choose those R_i−R_j that showed at least one atom inside a radius (r) equal to 8.0 Å. Thus, R_i and R_j were decomposed into individual fragments by cutting through the peptide bonds, and a pair of conjugate caps is designed to saturate each fragment, aiming to preserve the local chemical environment and comply with the valence requirements. Finally, hydrogen atoms are added into the molecular caps to avoid dangling bonds.[44] Here, the caps are formed by the neighbor residue covalently bound to the amine (C_i and C_j) and carboxyl (C_{i*} and C_{j*}) groups of residues R_i and R_j, respectively, along the protein chain, providing a better description of its electronic environment. Finally, the interaction energy (IE) of each residue−residue pair, IE(R_i−R_j), was calculated as follows

$$\mathrm{IE}(R_{ij}) = E(\Delta_{ij}) - E(\Delta_i - \delta_j) - E(\delta_i - \Delta_j) + E(\delta_{ij}) \quad (1)$$

where $\Delta_m = C_m R_m C_{m*}$, and $\delta_m = C_m C_{m*}$ ($m = i, j$). The term $E(\Delta_{ij})$ corresponds to the total energy of the fragment comprised by both capped residues. The second [third] term, $E(\Delta_i - \delta_j)$ [$E(\delta_i - \Delta_j)$], gives the total energy of the system formed by the capped residue R_i [R_j] and the hydrogenated caps of R_j [R_i]. $E(\delta_{ij})$ is the total energy of the system formed only by the caps. Additionally, in order to achieve the structural stability of the complex promoted by interactions with the extended hydration network, all water molecules forming hydrogen bonds with a particular residue or cap were included for completeness in the fragments. The

https://doi.org/10.1021/acs.jcim.1c01544
J. Chem. Inf. Model. XXXX, XXX, XXX−XXX

descriptions of the interaction types were obtained through the Discovery Studio visualizer[45] and visual inspection.

RESULTS AND DISCUSSION

In this work, the quantum mechanical calculations were employed to describe the residue−residue interactions and highlight the hot spot on the proteins' surface. This is a valuable strategy in drug design due to its potential for the identification of druggable sites. Thus, it can lead to the development of new therapeutic strategies to modulate this system under pathological conditions. Seeking a detailed understanding of the residue−residue network supporting the hACE-2 and S protein interaction, a total of 62, 63, and 54 residues belonging to hACE-2 and 51, 49, and 27 residues belonging to spike proteins were considered, resulting in 357, 333, and 276 interaction pairs evaluated for the complex hACE-2/spike of SARS-CoV-2, SARS-CoV, and HCoV-NL63, respectively.

By adding the interaction energies (IE) for all R_i−R_j within r = 8.0 Å,[46] we obtained the total interaction energies (TIEs) between the hACE-2 and spike proteins as −118.6, − 83.1, and −64.6 kcal mol^{-1} for the SARS-CoV-2, SARS-CoV, and HCoV-NL63 complexes, respectively, which is in accordance with the experimental order.[14,17−20,47] It is also in agreement with the observations of Rawat et al., where the authors obtained a positive correlation between the interaction surface size, the interaction energy, and the increased virulence of CoVs.[48] A list with all calculated interaction energies for individual residues is shown in Tables S1−S6 in the Supporting Information. From now on, SARS-CoV-2, SARS-CoV, and HCoV-NL63 are termed SARS-2, SARS, and NL63, respectively, and all the energy values are in kcal mol^{-1}.

Energetic Description of Secondary Structures. It has been shown that SARS-CoV-2 and SARS-CoV receptor-binding domains (RBDs) share approximately 72% amino-acid sequence identities, while the comparison with HCoV-NL63 is quite low (∼23%−25%).[48] Similarly, the structures of the RBDs from both SARS-CoVs are analogous when compared to each other but different when compared to HCoV-NL63.[23] In Figure 1 (top), we present the structures of the SARS (Figure 1(a)), SARS-2 (Figure 1(b)), and NL63 (Figure 1(c)) RBDs. As one can see, the three S protein-RBD contains two subdomains: a core structure and the receptor-binding motif (RBM). The core structures of SARS (Figure 1(a); orange) and SARS-2 (Figure 1(b); yellow) consist of a five-stranded antiparallel β-sheet (β1, β2, β3, β4, and β7) and some short α-helices connecting them, while the NL63 (Figure 1(c); light pink) core structure is a β-sandwich consisting of two β-sheet layers (β5, β7, β8, β6, β3, and β4, β1, β2). The RBM of both SARS-CoVs are made of loops divided by two antiparallel β-strands, with approximately 70 amino acids that connect the β4−β7 in the core regions. On the other hand, NL63 RBM is formed by three small loops that connect the core β-sheets: β1−β2, β4−β5, and β7−β8. Besides, it can be seen that SARS RBD has some small differences in structures when compared to SARS-2, with the first presenting less defined secondary structures (α-helix or β-strand). These differences are reflected in the binding surface with hACE-2 and can be related to the specific recognition pattern of each CoV, as one can see in Figure 1 (bottom).

Several authors[6,49−51] have stated that the interactions between hACE-2 and S proteins occur in two main hot spots of hACE-2 that are in close contact with RBM: (i) One is in the α-helix 1 (α1). (ii) The other is in the region formed by the β-strands 3 and 4 (β3−β4). In order to analyze the energy relevance of these two hot spots, as well as looking for new ones, we analyzed the energetic profile of each secondary structure of both proteins to identify the most relevant ones. We summed the IEs between the amino-acid residues of hACE-2 and S proteins, separated by segments, and show the results in Figure 2.

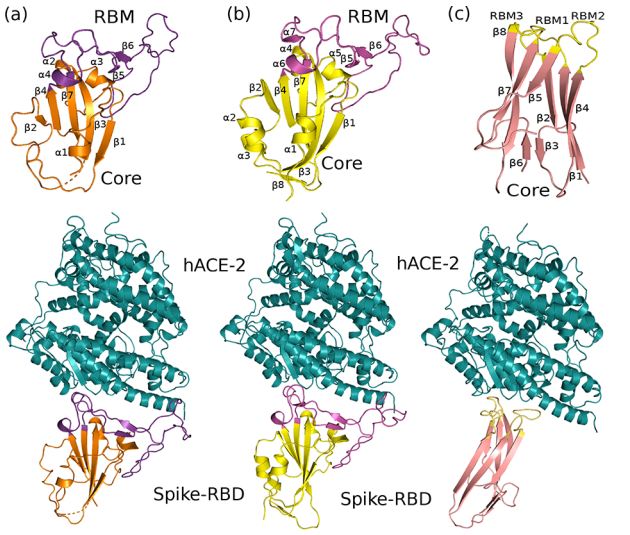

Figure 1. Overall structures of (a) SARS-CoV, (b) SARS-CoV-2, and (c) HCoV-NL63 RBD (top), each complexed with their common receptor, hACE-2 (botom). Core regions of RBDs are in orange (SARS), yellow (SARS-2), and light pink (NL63) colors, while RBMs of SARS, SARS-2, and NL63 are in purple, pink, and yellow, respectively.

As one can see in Figure 2(a), three segments of hACE-2 (yellow color) are recognized with the strongest interaction energy by all the CoVs here studied, name as α-helix α1 (SARS, −43.9, SARS-2, −72.3, NL63, −20.9), beta-sheet β4 (SARS, 4.9, SARS-2, −4.5, NL63, −3.4), and loop L18 (SARS, −13.7, SARS-2, −26.8, NL63, −22.1), which is in agreement with the previous studies. Here, it is noticeable that the amino acids of SARS-2 in the crystal structures are more tightly bound to these segments than the other two CoVs, mainly with the α1, which accounts for 179, 220, and 68 of all interaction pairs evaluated in hACE-2/SARS, SARS-2, and NL63 complexes, respectively, indicating that this segment could be a good starting point in the development of inhibitors to the viral docking in hACE-2. Besides, each one of the CoVs also showed a strong interaction with a specific region of the host's target compared to the other viruses. The segment α14 (pink color) presents more favorable interactions for SARS (−18.0) spike proteins than the other two viruses, while the interaction with SARS-2 (−3.9) and NL63 (−3.4) were weaker and quite similar to each other. L3 (purple color) amino acids are not forming an interaction with NL63 residues, but they are attracted by SARS-2 (−5.8) and repelled by some SARS (3.0) residues. Finally, the loops L16 (SARS, −0.6, SARS-2, −0.5, NL63, −6.5) and L20 (SARS, −0.4, SARS-2, −0.5, NL63, −4.7) (orange color) are specific recognition regions of the NL63 virus.

Figure 2(b) and (c) depicts the segments of both SARS-CoVs and NL63 spike proteins that are interacting with hACE-2 residues, respectively. As observed for hACE-2 segments, Figure 2(b) shows that the interaction energy between hACE-

https://doi.org/10.1021/acs.jcim.1c01544
J. Chem. Inf. Model. XXXX, XXX, XXX−XXX

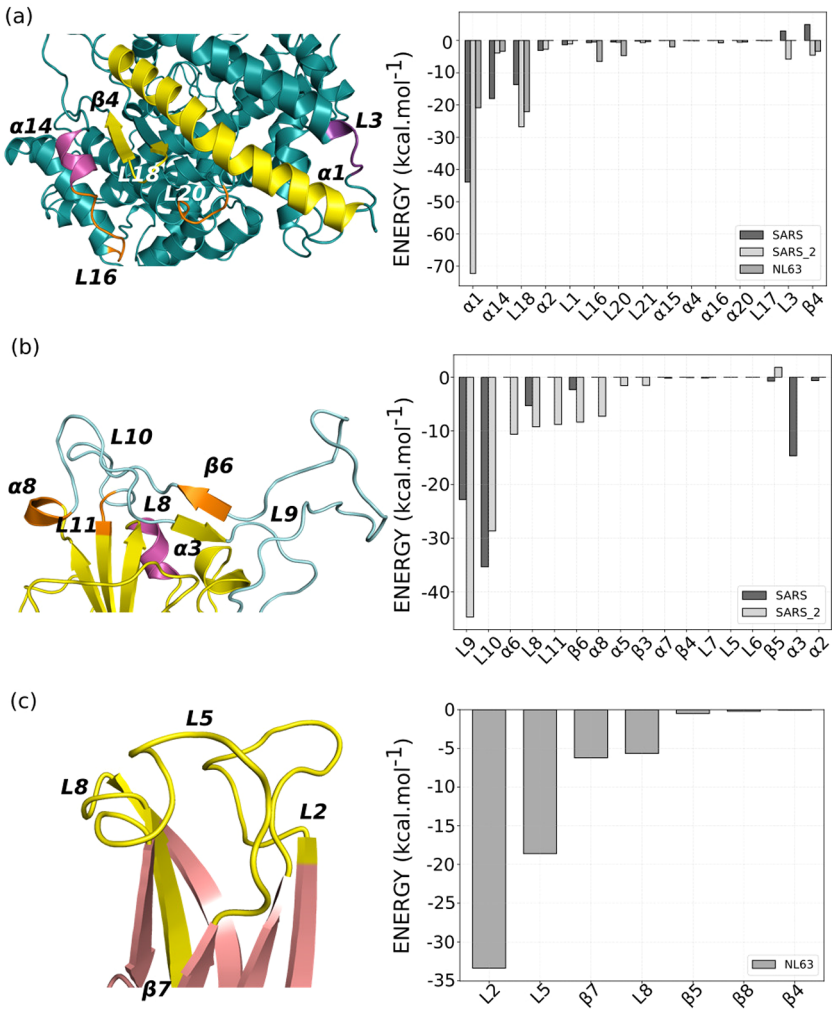

Figure 2. Interaction energies per (a) hACE-2, (b) SARS and SARS-2, and (c) NL63 protein secondary structures. In the left panel, we give a view about protein structures. In panel (a), the yellow color represents a common binding site for the three proteins. The orange color is a binding site exclusively for NL63. The pink region is a binding site only for SARS. The purple is the SARS-2 exclusive site.

2 and the S protein of SARS-2 is stronger than SARS in most of the segments, except the α-helix 3 (α3) and loop 10 (L10). As expected, the two segments with the strongest interaction energies are at the top of RBM (L9 and L10), closer to the receptor. It should be mentioned that the numbering in S protein α-helices is not exactly the same for SARS and SARS-2, as SARS has a more disordered structure, and some helices are not formed (Figure 1; top). This disordered, and consequently more flexible, characteristic has been pointed out as one of the factors for the lower affinity between the spike of SARS and hACE-2 in comparison to SARS-2 and can be related to a small binding surface.[48] In Figure 2(c), one can see the most relevant segments of NL63. From this, it is possible to realize that almost all the amino acids interacting with the human receptor are in the three loops of the virus RBM, except β7.

These results reinforce the relevance of the spike protein RBM residues, as well as the segments formed by the helix α1 and the β-turn "β3-L18-β4" in hACE-2 for the attachment of CoVs to the host's protein. Moreover, we found segments of both proteins that seem to be specific for the recognition of each virus, including the α-helix 3 of SARS, the segments α14, L3, L16, and L20 of hACE-2, and the β-strand 7 of NL63.

Hot-Spot Region between hACE-2 and CoVs S Protein. It is of great interest to identify the dominant sets of contact residues involved in attraction or repulsion between hACE-2 and S proteins. In order to evaluate this interaction in different species of coronaviruses, we performed a search for the most relevant residue−residue pair interactions. Figure 3 depicts the 24 residues of hACE-2 in which the sum of the interaction energies with all other residues belonging to the spike within a radius of 8.0 Å showing an energy value stronger than 2.0 or −2.0 kcal mol^{-1} at least in one of the three complexes studied. One can see that the residues $Q24_{ACE2}$, $T27_{ACE2}$, $F28_{ACE2}$, $D30_{ACE2}$, $K31_{ACE2}$, $H34_{ACE2}$, $E37_{ACE2}$, $D38_{ACE2}$, $Y41_{ACE2}$, $Q42_{ACE2}$, and $L45_{ACE2}$ contribute with about 48% (− 42.2), 69% (− 70.4), and 37% (− 19.0) of the TIEs of hACE-2 interacting with SARS (− 87.6), SARS-2 (− 101.3), and NL63 (− 50.3) spike proteins, respectively. It explains the reason for the hACE-2 α1 segment being the most important region of the protein, in terms of interaction energy, since these residues are part of this secondary structures. From these residues, only $Y41_{ACE2}$ show energetically relevant results, using the energy criterion above, for all the three complexes, while $D30_{ACE2}$, $H34_{ACE2}$, and $E37_{ACE2}$ are strongly bond to NL63 and only one of the SARS viruses (SARS or SARS-2). The residues $Q24_{ACE2}$, $T27_{ACE2}$, $F28_{ACE2}$, $K31_{ACE2}$, $D38_{ACE2}$, and $L45_{ACE2}$ present strong total interaction energies with both SARS and SARS-2 spike residues, while $Q42_{ACE2}$ is only

https://doi.org/10.1021/acs.jcim.1c01544
J. Chem. Inf. Model. XXXX, XXX, XXX−XXX

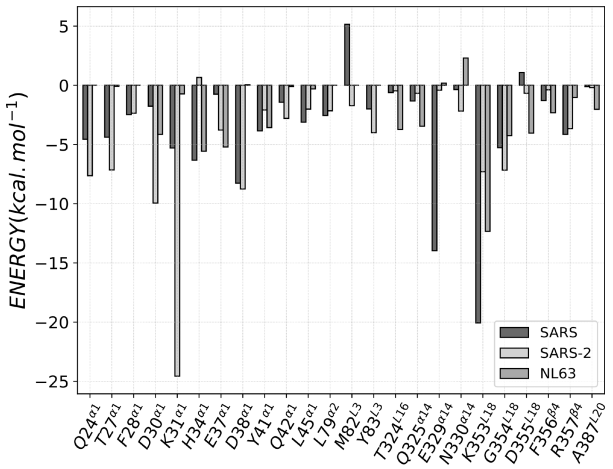

Figure 3. Energy profiles for the hACE-2 amino-acid residues with strongest interaction energies in the recognition surface interacting with amino acids from spike proteins within a radius of 8.0 Å. Here, we use a gray scale with dark gray, light gray, and gray represents SARS, SARS-2, and NL63 energy spectra, respectively.

energetically relevant to the hACE-2/SARS-2 complex (see the energy values for the three complexes in Table 1).

Table 1. Total Interaction Energy Values of Each One of the Most Relevant Residues of hACE-2 in Complex with Spike Proteins of SARS, SARS-2, and NL63

	Energy (kcal mol^{-1})		
Residues	SARS	SARS-2	NL63
Y41$^{\alpha1}$	−3.9	−2.1	−3.6
D30$^{\alpha1}$	−1.8	−9.9	−4.1
H34$^{\alpha1}$	−6.3	0.7	−5.6
E37$^{\alpha1}$	−0.8	−3.8	−5.2
Q24$^{\alpha1}$	−4.6	−7.6	0.0
T27$^{\alpha1}$	−4.4	−7.2	−0.1
F28$^{\alpha1}$	−2.5	−2.4	0.0
K31$^{\alpha1}$	−5.3	−24.6	−0.7
D38$^{\alpha1}$	−8.3	−8.8	0.1
L45$^{\alpha1}$	−3.1	−2.0	−0.3
Q42$^{\alpha1}$	−1.4	−2.8	−0.1
L79$^{\alpha2}$	−2.6	−2.2	0.0
M82^{L3}	5.2	−1.7	0.0
Y83^{L3}	−2.0	−4.0	0.0
T324^{L16}	−0.6	−0.5	−3.7
Q325$^{\alpha14}$	−1.3	−0.7	−3.5
E329$^{\alpha14}$	−14.0	−0.4	0.2
N330$^{\alpha14}$	−0.4	−2.2	2.3
K353^{L18}	−20.1	−7.3	−12.3
G354^{L18}	−5.3	−7.2	−4.3
D355^{L18}	1.1	−0.7	−4.0
F356$^{\beta4}$	−1.3	−0.4	−2.3
R357$^{\beta4}$	−4.1	−3.7	−1.0
A387^{L20}	−0.1	−0.2	−2.0

As one can see, there are not any other hACE-2 segments with more than three energetically relevant residues. Therefore, we present all the other ones here, and the values are listed in Table 1 for $L79_{ACE2}{}^{\alpha2}$, $M82_{ACE2}{}^{L3}$, $Y83_{ACE2}{}^{L3}$, $T324_{ACE2}{}^{L16}$, $Q325_{ACE2}{}^{\alpha14}$, $E329_{ACE2}{}^{\alpha14}$, $N330_{ACE2}{}^{\alpha14}$, $K353_{ACE2}{}^{L18}$, $G354_{ACE2}{}^{L18}$, $D355_{ACE2}{}^{L18}$, $F356_{ACE2}{}^{\beta4}$, $R357_{ACE2}{}^{\beta4}$, and $A387_{ACE2}{}^{L20}$. From these, only $K353_{ACE2}$ and $G354_{ACE2}$ are shown to be energetically relevant for the three complexes, while $T324_{ACE2}$, $Q325_{ACE2}$, $D355_{ACE2}$, $F356_{ACE2}$, and $A387_{ACE2}$ are strongly bound to NL63, as well as $L79_{ACE2}$ and $R357_{ACE2}$ present strong total interaction energies with both SARS viruses. Similarly, in Figure 4, one can see the most energetically relevant amino acids of SARS, SARS-2, and NL63 spike proteins, named as **SARS** $R426_{Spike}{}^{\alpha3}$, $Y436_{RBD}{}^{L8}$, $L442_{RBD}{}^{L9}$, $P462_{RBD}{}^{L9}$, $N473_{RBD}{}^{L9}$, $Y475_{RBD}{}^{L9}$, $N479_{RBD}{}^{\beta6}$, $Y484_{RBD}{}^{L10}$, $T486_{RBD}{}^{L10}$, $T487_{RBD}{}^{L10}$, $I489_{RBD}{}^{L10}$, and $Y491_{RBD}{}^{L10}$; **SARS-2** $K417_{RBD}{}^{\alpha6}$, $Y449_{RBD}{}^{L8}$, $Y453_{RBD}{}^{\beta5}$, $F456_{RBD}{}^{L9}$, $A475_{RBD}{}^{L9}$, $E484_{RBD}{}^{L9}$, $F486_{RBD}{}^{L9}$, $N487_{RBD}{}^{L9}$, $Y489_{RBD}{}^{L9}$, $Q493_{RBD}{}^{\beta6}$, $G496_{RBD}{}^{L10}$, $Q498_{RBD}{}^{L10}$, $T500_{RBD}{}^{L10}$, $N501_{RBD}{}^{L10}$, $G502_{RBD}{}^{\alpha8}$, and $Y505_{RBD}{}^{L10}$; **NL63** $G494_{RBD}{}^{L2}$, $S496_{RBD}{}^{L2}$, $C497_{RBD}{}^{L2}$, $Y498_{RBD}{}^{L2}$, $V499_{RBD}{}^{L2}$, $S535_{RBD}{}^{L5}$, $P536_{RBD}{}^{L5}$, $G537_{RBD}{}^{L5}$, $W585_{RBD}{}^{\beta7}$, and $H586_{RBD}{}^{L8}$ (see Table S7 to observe the total interaction energy values of each one of these residues).

These results are well correlated with previous experimental and computational data.[23,51−70] Spinello et al. performed a multimicrosecond-long molecular dynamics simulations over the structures of SARS-CoV(−2)/ACE2 and SARS-CoV/ACE2 complexes, observing that regions of spike protein of SARS-CoV-2/ACE2 are markedly more rigid as compared to SARS-CoV, as well as they revealed a map of the most important H-bond and salt bridge interactions that enable it to be more stable.[51] Important studies using fragment molecular orbitals were carried out to characterize the protein−protein interactions (PPI) between RBD and several antibody/peptides[52] as well as PPI in the RBD-hACE2 interfaces.[56] In the former, nine key residues were found in RBD (T415, K417, Y421, F456, A475, F486, N487, N501, and Y505), while in the latter, four residues (E37, K353, G354, and D355) of the hACE2 were identified as forming strong interactions with the spike proteins of coronaviruses (SARS-CoV-1, SARS-CoV-2, and HCoV-NL-63). Through mutagenesis study, Yi et al. reported that mutations in the SARS RBD residues R426, K439, N457, P470, Y484, T487, and Y491 decreased dramatically its binding affinities to the hACE-2, while by replacing the SARS-2-RBD amino acids, N501, Q498, E484, T470, K452, and R439 were responsible for a decrease in its receptor binding affinity. Interesting, the residues $K439_{RBD}$ and $N457_{RBD}$ of SARS, as well as $T470_{RBD}$, $K452_{RBD}$, and $R439_{RBD}$ of SARS-2, are not present in our 8.0 Å radius, indicating that their relevance is not related to the direct interaction with hACE-2.[71]

Zou et al. performed a molecular dynamics simulation together with an alanine scanning analysis, finding that relative binding free energy of the hACE-2/SARS complex is significantly changed when there is a mutation in the spike residues R426, L443, Y484, and T487. In our work, $L443_{RBD}$ is only making one interaction pair with IE over −1.0 kcal mol^{-1}, with hACE-2 residue $T27_{ACE2}$, and perhaps it is an interaction that was not captured by only taking into account a static crystal structure. Similarly, in the same work, it was shown that a mutation in the amino acid L455 of the S protein of SARS-2 resulted in the highest difference in binding energy, but in our outcomes, it presented only three weak IEs. Moreover, Zou et al. found the residues F456, F486, Q493, and N501 as the most relevant for the binding energy of the hACE-2/SARS-2 complex, which are also among the most relevant residues accordingly the herein reported results (Figure 4b).[72]

It is important to mention that mutations in spike residues K417(N/T), E484(K), and N501(Y) have been found in some

https://doi.org/10.1021/acs.jcim.1c01544
J. Chem. Inf. Model. XXXX, XXX, XXX−XXX

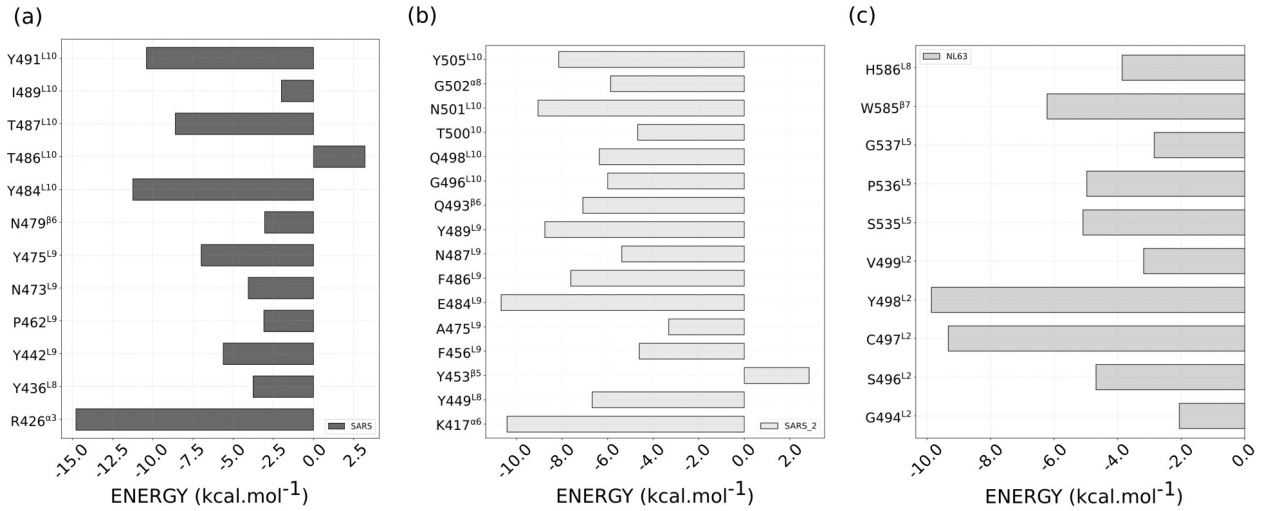

Figure 4. Energy profiles for (a) SARS, (b) SARS-2, and (c) NL63 spike amino-acid residues with strongest interaction energies in the recognition surfaces.

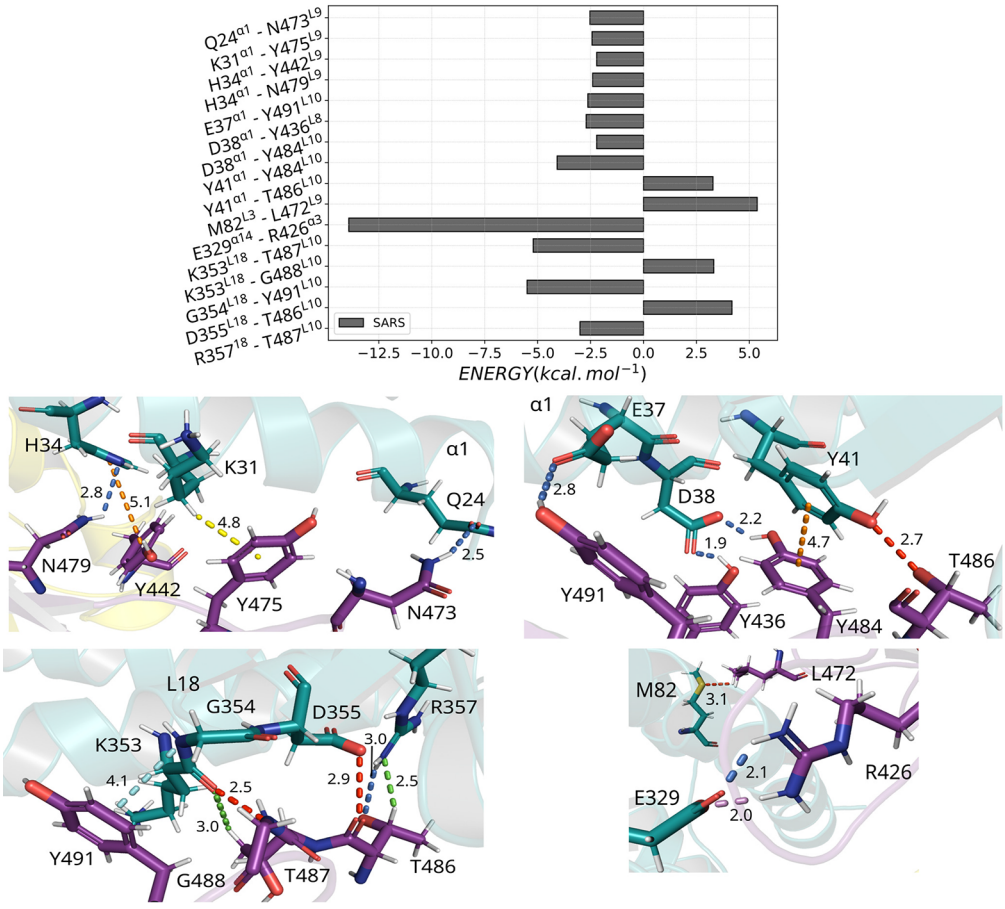

Figure 5. (Top) Graphical panel presenting the most relevant interactions involving the hACE-2−spike residues of SARS. (Bottom) Detailed spatial organization of the interaction pairs with their intermolecular interactions. Dashed lines in marine (green) represent direct (nonconventional) hydrogen bonds and orange (yellow) lines $\pi-\pi$ (π−alkyl). Repulsion, amide-π stacked, and salt bridges are represented in red, cyan, and violet lines, respectively.

SARS-2 variants, possibly involved in reducing neutralization by some antibodies.[66,67,69,70,73] From these, N501Y is present in lineages B.1.1.7 (Alpha), B.1.351 (Beta), and P.1 (Gamma), and E484K was observed in lineages Beta and Gamma, which also possess alternative amino-acid substitutions K417N and K417T, respectively. Watanabe et al.,[66] using the fragment molecular orbital method, found the K417N/T, E484K, and N501Y mutations are energetically disadvantageous for antibody interactions. Watanabe et al.[67] presented a detailed study on the N501Y mutation effect. They have concluded that this mutation on the S protein enhanced the attractive interaction in comparison to the wild S protein due to the

https://doi.org/10.1021/acs.jcim.1c01544
J. Chem. Inf. Model. XXXX, XXX, XXX−XXX

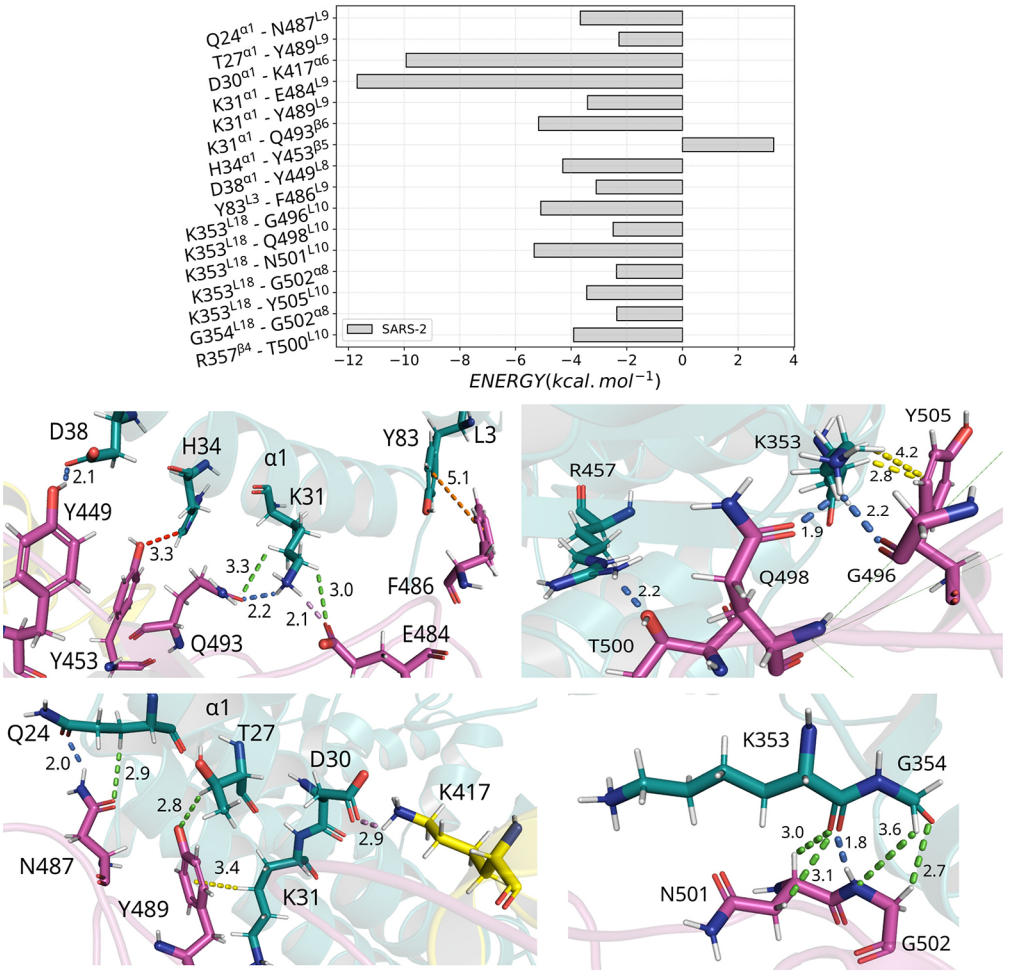

Figure 6. (Top) Graphical panel presenting the most relevant interactions involving the hACE-2−spike residues of SARS-2. (Bottom) Detailed spatial organization of the interaction pairs with their intermolecular interactions. Dashed lines in marine (green) represent direct (nonconventional) hydrogen bonds and orange (yellow) lines $\pi-\pi$ (π−alkyl). Repulsion and salt bridges are represented in red and violet lines, respectively.

hydrogen bonds and XH/*pi* interactions with Y41 and K353 from hACE-2.

Here, K417, E484, and N501 have shown some of the strongest attractive TIEs, and a study by Taka et al. depicted that spike residues E484 and K417 are involved in salt bridges with the hACE-2 residues K31 and D30, respectively, during most of the time of their molecular dynamics simulation,[74] which could help to understand the key role of these residues.[74] On the other hand, the mutation E484(K) leads to a small increase in the binding affinity of the complex,[75] and some computational studies have related it to a repulsive energy of E484, which is not present when the lysine residue is in position.[70,76,77] In our calculations, we only found one repulsion between $E484_{RBD}$ and a hACE-2 residue (Table S2), and it showed a quite small IE. This difference in the interaction energy could be related to the pose captured by the crystal structure, which represents a moment with favorable interactions, or to distinction in the calculation methods used.

On the other hand, there are only a few studies trying to understand the binding of hACE-2 to the NL63 S protein at a molecular level, as well as the effects of mutations in hACE-2 for recognizing CoVs.[17,18,23,78] Wu et al. reported four mutations in hACE-2 (K353A, D38A, D37A, Y41A, and Y41F) that decrease the binding affinity for NL63 and the SARS S protein, as well as three NL63 spike mutations (Y498A, S535A, and S535T).[47] Rawat et al. studied the conserved residues in the spike protein by *in silico* analysis, showing that the conserved glycine and tyrosine residues in SARS (G488 and Y436), SARS-2 (G502 and Tyr449), and NL63 (G537 and Y498) are important for both stabilizing the S protein and its interaction with hACE-2.[48] It has been depicted by Li et al. that nine mutations in hACE-2 affected inhibition of interactions with SARS (Q24K, K31D, Y41A, K68D, K353D, K353A, D255A, R357A, and R393A).[65]

Finally, to assess the differences in the interactions between hACE-2 and the S protein of the three coronaviruses, we performed a thorough analysis of the individual interaction pairs. All energy values are in kcal mol^{-1}. In Figures 5−7 (top), we present the most energetically relevant interaction pairs in the complexes hACE-2 with SARS (Figure 5), SARS-2 (Figure 6), and NL63 (Figure 7), respectively. Among the 11 hACE-2 α1 residues, $Y41_{ACE2}$ forms interaction pairs with 14, 13, and 7 residues of SARS, SARS-2, and NL63, respectively, but most of the IE values are weakly attractive (negative). When the energy criterion is applied ($\geq$2.0 kcal mol^{-1} or ≤ -2.0 kcal mol^{-1}), 2 (SARS), 0 (SARS-2), and 1 (NL63) interaction pairs are observed. In the complex hACE-2/SARS, the two strongest IEs of $Y41_{ACE2}$ are with the residues $Y484_{RBD}$ ($Y41_{ACE2}{}^{\alpha 1}-$

https://doi.org/10.1021/acs.jcim.1c01544
J. Chem. Inf. Model. XXXX, XXX, XXX−XXX

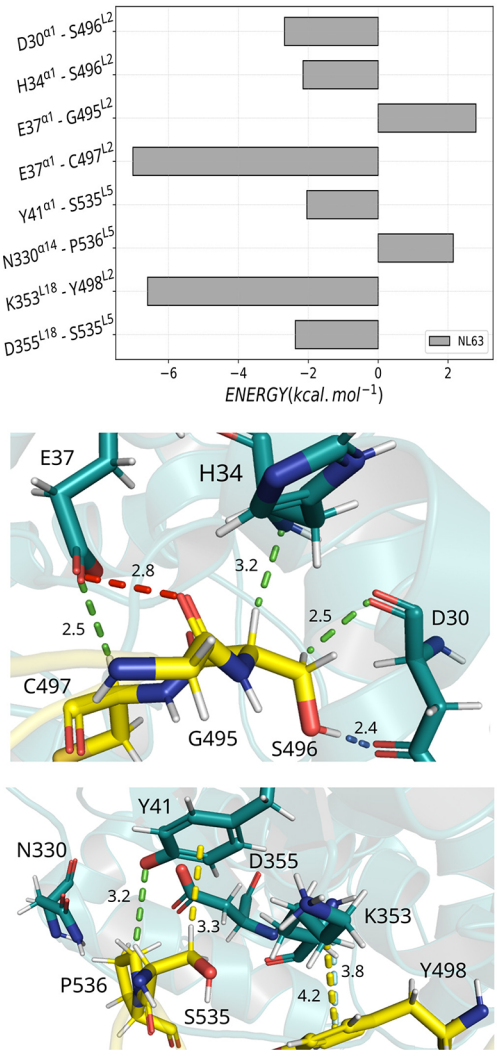

Figure 7. (Top) Graphical panel presenting the most relevant interactions involving the hACE-2−spike residues of NL63. (Bottom) Detailed spatial organization of the interaction pairs with their intermolecular interactions. Dashed lines in marine (green) represent direct (nonconventional) hydrogen bonds and orange (yellow) lines $\pi-\pi$ (π−alkyl). Rrepulsion, amide-π stacked, and salt bridges are represented in red, cyan, and violet lines, respectively.

$Y484_{RBD}{}^{L10}$: −4.1) and $T486_{RBD}$ ($Y41_{ACE2}{}^{\alpha1}-T486_{RBD}{}^{L10}$: 3.3) through the formation of a $\pi-\pi$ interaction (4.7 Å) and a repulsion between the oxygen atoms from their side-chain hydroxyl groups (distant 2.73 Å from each other), respectively. Looking for these IEs, $Y41_{ACE2}$ is not expected to be among those residues with the strongest interaction energy, but it is also in an π−alkyl interaction (4.0 Å) with $T487_{RBD}$ ($Y41_{ACE2}{}^{\alpha1}-T487_{RBD}{}^{L10}$: −1.5) that increases the attraction between the hACE-2 residue and S protein.

$Y41_{ACE2}$ does not have any individual interaction with spike residues of SARS-2 within the energy criterion, but three interaction pairs are the main ones responsible for the energy of this residue to be within the criterion (all other energy values can be seen in Table S2): $Y41_{ACE2}{}^{\alpha1}-Q498_{RBD}{}^{L10}$ (−2.0), $Y41_{ACE2}{}^{\alpha1}-T500_{RBD}{}^{L10}$ (1.9), and $Y41_{ACE2}{}^{\alpha1}-N501_{RBD}{}^{L10}$ (−1.0). The first attraction occurs by a nonconventional hydrogen bond (from now on, nonconventional H-bond) between the amine side chain of the glutamine and a C−H group from the tyrosine ring (2.60 Å), while the second attraction is the result of small hydrophobic contacts between the amino acids. Curiously, $T500_{RBD}$ in SARS-2 occupies the same position as $T486_{RBD}$ in the SARS S protein, and both residues are involved in repulsion with $Y41_{ACE2}$ through the oxygen atoms from their side-chain hydroxyl groups in a similar distance (2.9 Å). On the other hand, S535 ($Y41_{ACE2}{}^{\alpha1}-S535_{RBD}{}^{L5}$) of NL63 interacts with hACE-2 $Y41_{ACE2}$ through a nonconventional H-bond (3.2 Å) and a π−alkyl interaction (3.3 Å) with an IE of −2.1.

As one can see in Figure S1(a), SARS $Y484_{ACE2}$ and $T487_{ACE2}$ are almost overlapping the positions of SARS-2 $Q498_{ACE2}$ and $N501_{ACE2}$, respectively, while the NL63 $S535_{ACE2}$ main chain is quite close to the position of $T487_{ACE2}$ (with the side chain rotating to the other side; Figure S1(b)), indicating that the presence of hydrophobic or small polar residues surrounding hACE-2 $Y41_{ACE2}$ is more favorable to the stabilization of the spike protein, although the repulsion to $T486_{ACE2}$ and $T500_{ACE2}$ should also be considered. These results explain the more energetic behavior of the SARS-RBD loop 10 ($L10$) when compared to SARS-2.

The residues $Q24_{ACE2}{}^{\alpha1}$, $K31_{ACE2}{}^{\alpha1}$, $D38_{ACE2}{}^{\alpha1}$, and $G354_{ACE2}{}^{L18}$ are the hACE-2 residues that showed IEs within energy criterion and that only interacted with SARS and SARS-2 residues. The position of $Q24_{ACE2}$ is almost overlapped in both crystals (Figure S1(c)), as well as the positions of $N473_{RBD}{}^{L9}$ and $N487_{RBD}{}^{L9}$ of SARS and SARS-2 spike, respectively (Figure S1(d)). These amino acids are making H-bonds with $Q24_{ACE2}$ and show IEs of −2.5 ($Q24_{ACE2}{}^{\alpha1}-N473_{RBD}{}^{L9}$; 2.5 Å) and −3.7 ($Q24_{ACE2}{}^{\alpha1}-N487_{RBD}{}^{L9}$: 2.0 Å). Besides, the interaction pair $Q24_{ACE2}{}^{\alpha1}-N487_{RBD}{}^{L9}$ also presented a nonconventional H-bond at a distance of 2.9 Å. $K31_{ACE2}$ is an important residue for SARS-2 interactions, accounting for three strong interaction pairs with $E484_{RBD}$ ($K31_{ACE2}{}^{\alpha1}-E484_{RBD}{}^{L9}$: −11.7), $Y489_{RBD}$ ($K31_{ACE2}{}^{\alpha1}-Y489_{RBD}{}^{L9}$: −3.4), and Q493 ($K31_{ACE2}{}^{\alpha1}-Q493_{RBD}{}^{\beta6}$: −5.2). The first pair is the second strongest IE and is making a salt bridge (2.1 Å) and a nonconventional H-bond (3.1 Å), while the second is involved in a π−alkyl (4.4 Å) and several hydrophobic interactions, and finally, in the third pair, there is an H-bond (2.2 Å) and a nonconventional H-bond (3.3 Å) being made. In contrast, in the position occupied by the residue $Y489_{RBD}$ (SARS-2), there is the amino acid $Y475_{RBD}{}^{L9}$ in SARS, and it is also making a π−alkyl interaction with K31 ($K31_{ACE2}{}^{\alpha1}-Y475_{RBD}{}^{L9}$: −2.4) at a distance of 3.6 Å.

Moreover, the residue $D38_{ACE2}$ seems to be relevant to SARS, since it has two interaction pairs with spikes $Y436_{RBD}$ ($D38_{ACE2}{}^{\alpha1}-Y436_{RBD}{}^{L8}$: −2.7) and $Y484_{RBD}$ ($D38_{ACE2}{}^{\alpha1}-Y484_{RBD}{}^{L10}$: −2.2) residues, both of them making H-bonds at distances of 1.9 and 2.2 Å, respectively. On the other hand, in the complex SARS-2/hACE-2, $D38_{ACE2}$ makes an H-bond with residue $Y449_{RBD}{}^{L8}$ ($D38_{ACE2}{}^{\alpha1}-Y449_{RBD}{}^{L8}$; 2.1 Å), showing an IE of −4.3. It is important to note that the SARS residue $Y436_{RBD}$ is overlapping the residue $Y449_{RBD}$ of SARS-2 (Figure S1(a)), indicating the relevance of the presence of an H-bond with the residue $D38_{ACE2}$ of hACE-2 for both SARS-CoVs. Finally, the interaction pairs in SARS $G354_{ACE2}{}^{L8}-Y491_{RBD}{}^{L10}$ and SARS-2 $G354_{ACE2}{}^{L8}-G502_{RBD}{}^{\alpha8}$ have IEs of −5.5 (π−amide: 4.1 Å) and −2.4 (nonconventional H-bond: 2.7 Å; 3.6 Å), respectively.

Residue $D30_{ACE2}$ interacts with 8, 10, and 4 residues of SARS, SARS-2, and NL63, respectively, while 0, 1, and 1 interaction pairs have higher IEs than the energy criterion used. All IEs with the eight residues of SARS are below −0.9

https://doi.org/10.1021/acs.jcim.1c01544
J. Chem. Inf. Model. XXXX, XXX, XXX−XXX

kcal mol^{-1}; therefore, they will not be discussed here. On the other hand, in the complex hACE-2/SARS-2, the interaction pair D30$_{ACE2}{}^{\alpha1}$−K417$_{RBD}{}^{\alpha6}$ shows the third strongest IE (−9.9) of all complexes which occur by the formation of a salt bridge between their charged side chain (2.9 Å), while D30$_{ACE2}{}^{\alpha1}$−S496$_{RBD}{}^{L2}$ (NL63) forms an H-bond (2.4 Å) and a nonconventional H-bond (2.5 Å) with IEs of −2.7.

From the 19 (SARS), 17 (SARS-2), and 7 (NL63) interaction pairs of H34$_{ACE2}$ with S proteins, 2 (SARS), 1 (SARS-2), and 1 (NL63) are within the energy criterion. H34$_{ACE2}{}^{\alpha1}$−Y442$_{RBD}{}^{L9}$ (SARS) and H34$_{ACE2}{}^{\alpha1}$−N479$_{RBD}{}^{\beta6}$ (SARS) interaction pairs create a $\pi-\pi$ (5.1 Å) interaction and a H-bond (2.8 Å), with IEs of −2.2 and −2.4, respectively. The IE of H34$_{ACE2}{}^{\alpha1}$−Y453$_{RBD}{}^{\beta5}$ (SARS-2) is 3.3 with a repulsion between the C−N−C ring side chain and the hydroxyl oxygen (3.3 Å), and H34$_{ACE2}{}^{\alpha1}$−S496$_{RBD}{}^{L2}$ (NL63) forms a nonconventional H-bond (−2.2) at 3.2 Å.

The residue E37$_{ACE2}$ of hACE-2 is interacting with 9, 11, and 12 residues of SARS, SARS-2, and NL63 S proteins, respectively, but only in the last complex do we observe IE values within the energy criterion: E37$_{ACE2}{}^{\alpha1}$−G495$_{RBD}{}^{L2}$ with an IE of 2.8, through a repulsion between the oxygen atoms from the E37$_{ACE2}$ carboxyl group and G495 main chain (3.1 Å) and E37$_{ACE2}{}^{\alpha1}$−C497$_{RBD}{}^{L2}$ with IEs of −7.0 through a nonconventional H-bond (2.50) and some hydrophobic interactions. However, two residues of SARS-2, R403$_{RBD}{}^{\beta3}$ and Y505$_{RBD}{}^{L10}$, showed attractive interactions to hACE-2 E37$_{ACE2}$ close to −2.0 (−1.7 and −1.8, respectively).

Two residues of hACE-2 only show energetically relevant IE with the SARS complexes: M82$_{ACE2}{}^{L3}$ and E329$_{ACE2}{}^{\alpha14}$. The IE of M82$_{ACE2}$ with L472$_{RBD}$ has the strongest repulsion among the three complexes (M82$_{ACE2}{}^{L3}$−L472$_{RBD}{}^{L9}$: 5.4), being caused by the proximity between the sulfur atom of methionine and the methyl group of leucine (3.1 Å), while E329$_{ACE2}$ is interacting with R426$_{RBD}$ with the strongest attraction (E329$_{ACE2}{}^{\alpha14}$−R426$_{RBD}{}^{\alpha3}$: −13.9) through a salt bridge (2.0 Å) and an H-bond (2.1 Å). On the other hand, T27$_{ACE2}{}^{\alpha1}$ and Y83$_{ACE2}{}^{L3}$ are the residues of hACE-2 that formed strong interactions only with SARS-2. In the first, T27$_{ACE2}$ interacts with Y489$_{RBD}{}^{L9}$ through a nonconventional H-bond (T27$_{ACE2}{}^{\alpha1}$−Y489$_{RBD}{}^{L9}$: −2.3) at a distance of 2.8 Å, and in the second, Y83$_{ACE2}$ forms a $\pi-\pi$ (5.1 Å) interaction with F486$_{RBD}$ (Y83$_{ACE2}{}^{L3}$−F486$_{RBD}{}^{L9}$: −3.1). Finally, K353$_{ACE2}$ interacts strongly with the residues of SARS T487$_{RBD}$ (K353$_{ACE2}{}^{L18}$−T487$_{RBD}{}^{L10}$: −5.2) through a nonconventional H-bond (3.0 Å) and G488$_{RBD}$ (K353$_{ACE2}{}^{L18}$−G488$_{RBD}{}^{L10}$: 3.3) through a repulsion with the nitrogen in the main chain of G488 (2.5 Å), N501 (K353$_{ACE2}{}^{L18}$−N501$_{RBD}{}^{L10}$: −5.3) of SARS-2 through nonconventional H-bonds (3.0 and 3.1 Å) and with Y498$_{RBD}$ (K353$_{ACE2}{}^{L18}$−Y498$_{RBD}{}^{L2}$: −6.6) of NL63 by making a π-alkyl (4.2 Å) and an amide-π stacked (3.8 Å) interaction.

In summary, the overall receptor-binding modes of SARS and SARS-2 were quite similar, as well as the most energetically important residues of hACE-2 interacting with NL63, but the detailed interaction patterns were substantially different, which might explain the distinct affinities and immunogenic features. As one can see, the most relevant residues here presented are in agreement with published data, and new ones are shown, including I489$_{RBD}$, N473$_{RBD}$, and P462$_{RBD}$ (SARS), T500$_{RBD}$, Y489$_{RBD}$, and E484$_{RBD}$ (SARS-2), and H586$_{RBD}$, P536$_{RBD}$, and C497$_{RBD}$ (NL63). Finally, the strongest IE are seen by E329$_{ACE2}{}^{\alpha14}$−R426$_{RBD}{}^{\alpha3}$ (−13.9), G354$_{ACE2}{}^{L8}$−Y491$_{RBD}{}^{L10}$ (−5.5), Y41$_{ACE2}{}^{\alpha1}$−Y484$_{RBD}{}^{L10}$ (−4.1), and M82$_{ACE2}{}^{L3}$−L472$_{RBD}{}^{L9}$ (5.4) of SARS; K31$_{ACE2}{}^{\alpha1}$−E484$_{RBD}{}^{L9}$ (−11.7), D30$_{ACE2}{}^{\alpha1}$−K417$_{RBD}{}^{\alpha6}$ (−9.9), K353$_{ACE2}{}^{L18}$−N501$_{RBD}{}^{L10}$ (−5.3), and K31$_{ACE2}{}^{\alpha1}$−Q493$_{RBD}{}^{\beta6}$ (−5.2) of SARS-2; and E37$_{ACE2}{}^{\alpha1}$−C497$_{RBD}{}^{L2}$ (−7.0), K353$_{ACE2}{}^{L18}$−Y498$_{RBD}{}^{L2}$ (−6.6), D30$_{ACE2}{}^{\alpha1}$−S496$_{RBD}{}^{L2}$ (−2.68), and E37$_{ACE2}{}^{\alpha1}$−G495$_{RBD}{}^{L2}$ (2.8) of NL63.

CONCLUSION

Virus-receptor recognition is a primary phase that plays a decisive role in tissue tropism in host cells. Several studies have shown that SARS-CoV, SARS-CoV-2, and HCoV-NL63, despite binding to the same receptor, use fairly different mechanisms to recognize hACE-2 and initiate the cell entrance process that could be related to the order of binding affinity and severity of these viruses. In this sense, we employed quantum biochemistry methods to investigate the interactions of the hACE-2 with the spike protein of the three CoVs in atomic detail to understand the process by which these proteins interact, aiming to discover methods that could be used to neutralize virus infection.

According to the protein−protein interaction results, the total interaction energy between hACE-2 and spike protein obtained in this work followed the experimental binding affinity: SARS-2 (−118.6 kcal mol^{-1}) > SARS (−83.1 kcal mol^{-1}) > NL63 (−64.6 kcal mol^{-1}). In order to investigate the energetic relevance of the segments of both proteins to the attachment and search for differences among the CoV species, we observed that, as expected, the most important residues of hACE-2 are in the helix $\alpha1$ and the β-turn "$\beta3$-*L*18-$\beta4$", while in the S protein these residues are in the receptor-binding motif (RBM). Moreover, we found segments of both proteins that look to be specific for the recognition of each virus, including the α-helix 3 of SARS, the segments $\alpha14$, *L*3, *L*16, and *L*20 of hACE-2, and the β-strand 7 of NL63.

Finally, our results showed that 24 residues of hACE-2 are important to the recognition of the CoVs (Q24$_{ACE2}$, T27$_{ACE2}$, F28$_{ACE2}$, D30$_{ACE2}$, K31$_{ACE2}$, H34$_{ACE2}$, E37$_{ACE2}$, D38$_{ACE2}$, Y41$_{ACE2}$, Q42$_{ACE2}$, L45$_{ACE2}$, L79$_{ACE2}$, M82$_{ACE2}$, Y83$_{ACE2}$, T324$_{ACE2}$, Q325$_{ACE2}$, E329$_{ACE2}$, N330$_{ACE2}$, K353$_{ACE2}$, G354$_{ACE2}$, D355$_{ACE2}$, F356$_{ACE2}$, R357$_{ACE2}$, and A387$_{ACE2}$), while 12 (R426$_{RBD}$, T436$_{RBD}$, Y442$_{RBD}$, P462$_{RBD}$, N473$_{RBD}$, Y475$_{RBD}$, N479$_{RBD}$, Y484$_{RBD}$, T486$_{RBD}$, T487$_{RBD}$, L489$_{RBD}$, and Y491$_{RBD}$), 16 (K417$_{RBD}$, Y449$_{RBD}$, Y453$_{RBD}$, F456$_{RBD}$, A475$_{RBD}$, E484$_{RBD}$, F486$_{RBD}$, N487$_{RBD}$, Y489$_{RBD}$, Q493$_{RBD}$, G496$_{RBD}$, Q498$_{RBD}$, T500$_{RBD}$, N501$_{RBD}$, G502$_{RBD}$, and Y505$_{RBD}$), and 10 (G494$_{RBD}$, S496$_{RBD}$, C497$_{RBD}$, Y498$_{RBD}$, V499$_{RBD}$, S535$_{RBD}$, P536$_{RBD}$, G537$_{RBD}$, W585$_{RBD}$, and H586$_{RBD}$) residues are energetically relevant to the interaction of SARS, SARS-2, and NL63 with hACE-2, respectively. As one can see, the most relevant residues and segments here presented are in agreement with previous studies published during this two year period of the COVID-19 outbreak, as well as highlighting new ones: (a) segments α-helix 3 of SARS, $\alpha14$, *L*3, *L*16, and *L*20 of hACE-2, and the β-strand 7 of NL63, and (b) residues I489$_{RBD}$, N473$_{RBD}$, and P462$_{RBD}$ (SARS), T500$_{RBD}$, Y489$_{RBD}$, and E484$_{RBD}$ (SARS-2), and H586$_{RBD}$, P536$_{RBD}$, and C497$_{RBD}$ (NL63). These results provide valuable information for the discovery of antiviral therapeutics that inhibit protein−protein interactions of human pathogenic CoVs that use hACE-2 as a target.

https://doi.org/10.1021/acs.jcim.1c01544
J. Chem. Inf. Model. XXXX, XXX, XXX−XXX

DATA AND SOFTWARE AVAILABILITY

Structures used to perform the MFCC fragmentation are available in the Supporting Information. For the analysis of the results and plotting the energy data, we have used Python in-house scripts. Additional software details and data that support the findings of this study are available from the authors upon request.

ASSOCIATED CONTENT

Supporting Information

The Supporting Information is available free of charge at https://pubs.acs.org/doi/10.1021/acs.jcim.1c01544.

Figure S1: Overlapped molecular structure of amino acids in three complexes. Figure S2: Detailed view of the most relevant hACE-2/spike protein residue−residue interaction. Table S1: Detailed interaction energies of all amino acids that compose the binding site of hACE-2/spike protein (SARS-CoV) structure. Table S2: Detailed interaction energies of all amino acids that compose the binding site of hACE-2/spike protein (SARS-CoV-2) structure. Table S3: Detailed interaction energies of all amino acids that compose the binding site of hACE-2/spike protein (HCoV-NL63) structure. Table S4: Amino-acid residues of the interface of hACE-2/spike protein (SARS-CoV) for the interaction energy lower than 0.04 kcal mol^{-1}. Table S5: Amino-acid residues of the interface hACE-2/spike protein (SARS-CoV-2) for the interaction energy lower than 0.04 kcal mol^{-1}. Table S6: Amino-acid residues of the interface of hACE-2/spike protein (HCoV-NL63) for the interaction energy lower than 0.04 kcal mol^{-1}. Table S7: Total interaction energy values of each one of the most relevant residues of SARS, SARS-2, and NL63 S protein (PDF)

Input data used to perform MFCC fragmentation (ZIP)

AUTHOR INFORMATION

Corresponding Author

Umberto Laino Fulco − *Departamento de Biofísica e Farmacologia, Universidade Federal do Rio Grande do Norte, 59072-970 Natal-RN, Brazil;* orcid.org/0000-0002-4528-9878; Phone: +-55 (84) 3215-3419; Email: umbertofulco@gmail.com; Fax: +-55 (84) 3215-3791

Authors

José X. Lima Neto − *Departamento de Biofísica e Farmacologia, Universidade Federal do Rio Grande do Norte, 59072-970 Natal-RN, Brazil;* orcid.org/0000-0001-6428-811X

Davi S. Vieira − *Instituto de Química, Universidade Federal do Rio Grande do Norte, 59072-970 Natal-RN, Brazil*

Jones de Andrade − *Department of Physical Chemistry, Universidade Federal do Rio Grande do Sul, 91501-970 Porto Alegre-RS, Brazil*

Complete contact information is available at: https://pubs.acs.org/10.1021/acs.jcim.1c01544

Notes

The authors declare no competing financial interest.

ACKNOWLEDGMENTS

This work was supported by the Brazilian research agencies Conselho Nacional de Desenvolvimento Científico e Tecnológico - CNPq and the Coordenação de Aperfeiçoamento de Pessoal de Nível Superior - CAPES.

REFERENCES

(1) WHO Coronavirus (COVID-19) Dashboard, 2020. World Health Organization. https://covid19.who.int/ (accessed 02-November-2021).

(2) Lau, S. K.; Li, K. S.; Tsang, A. K.; Shek, C. T.; Wang, M.; Choi, G. K.; Guo, R.; Wong, B. H.; Poon, R. W.; Lam, C. S.; Wang, S. Y.; Fan, R. Y.; Chan, K. H.; Zheng, B. J.; Woo, P. C.; Yuen, K. Recent Transmission of a Novel Alphacoronavirus, Bat Coronavirus HKU10, from Leschenault's Rousettes to Pomona Leaf-Nosed Bats: First Evidence of Interspecies Transmission of Coronavirus between Bats of Different Suborders. *J. Virol.* **2012**, *86*, 11906−11918.

(3) Desforges, M.; Le Coupanec, A.; Dubeau, P.; Bourgouin, A.; Lajoie, L.; Dubé, M.; Talbot, P. J. Human Coronaviruses and Other Respiratory Viruses: Underestimated Opportunistic Pathogens of the Central Nervous System? *Viruses* **2020**, *12*, 14.

(4) Freitas, F. C.; Ferreira, P. H. B.; Favaro, D. C.; Oliveira, R. J. d. Shedding Light on the Inhibitory Mechanisms of SARS-CoV-1/CoV-2 Spike Proteins by ACE2-Designed Peptides. *J. Chem. Inf. Model.* **2021**, *61*, 1226−1243.

(5) Kumavath, R.; Barh, D.; Andrade, B. S.; Imchen, M.; Aburjaile, F. F.; Ch, A.; Rodrigues, D. L. N.; Tiwari, S.; Alzahrani, K. J.; Goes-Neto, A.; Weener, M. E.; Ghosh, P.; Azevedo, V. The Spike of SARS-CoV-2: Uniqueness and Applications. *Front. Immunol.* **2021**, *12*, 663912.

(6) Li, F. Receptor Recognition Mechanisms of Coronaviruses: A Decade of Structural Studies. *J. Virol.* **2015**, *89*, 1954−1964.

(7) Li, F. Structure, Function, and Evolution of Coronavirus Spike Proteins. *Annu. Rev. Virol.* **2016**, *3*, 237−261.

(8) Hasöksüz, M.; Kiliç, S.; Saraç, F. Coronaviruses and SARS-CoV-2. *Turk. J. Med. Sci.* **2020**, *50*, 549−556.

(9) Bian, J.; Li, Z. Angiotensin-Converting Enzyme 2 (ACE2): SARS-CoV-2 Receptor and RAS Modulator. *Acta Pharm. Sin. B* **2021**, *11*, 1−12.

(10) Jiang, F.; Yang, J.; Zhang, Y.; Dong, M.; Wang, S.; Zhang, Q.; Liu, F. F.; Zhang, K.; Zhang, C. Angiotensin-Converting Enzyme 2 and Angiotensin 1−7: Novel Therapeutic Targets. *Nat. Rev. Cardiol.* **2014**, *11*, 413.

(11) Xiang, Y.; Wang, M.; Chen, H.; Chen, L. Potential Therapeutic Approaches for the Early Entry of SARS-CoV-2 by Interrupting the Interaction between the Spike Protein on SARS-CoV-2 and Angiotensin-Converting Enzyme 2 (ACE2). *Biochem. Pharmacol.* **2021**, *192*, 114724.

(12) Maiti, B. K. Bioengineered Angiotensin-Converting Enzyme 2: A Potential Therapeutic Option against SARS-CoV-2 Infection. *J. Hum. Hypertens.* **2021**, 1−5.

(13) Samrat, S. K.; Tharappel, A. M.; Li, Z.; Li, H. Prospect of SARS-CoV-2 Spike Protein: Potential Role in Vaccine and Therapeutic Development. *Virus Res.* **2020**, *288*, 198141.

(14) Li, F. Evidence for a Common Evolutionary Origin of Coronavirus Spike Protein Receptor-Binding Subunits. *J. Virol.* **2012**, *86*, 2856−2858.

(15) Cueno, M.; Imai, K. Structural Comparison of the SARS-CoV-2 Spike Protein Relative to Other Human-Infecting Coronaviruses. *Front. Med.* **2020**, *7*, 594439.

(16) Tay, M. Z.; Poh, C. M.; Rénia, L.; MacAry, P. A.; Ng, L. F. The Trinity of COVID-19: Immunity, Inflammation and Intervention. *Nat. Rev. Immunol.* **2020**, *20*, 363−374.

(17) Mathewson, A. C.; Bishop, A.; Yao, Y.; Kemp, F.; Ren, J.; Chen, H.; Xu, X.; Berkhout, B.; van der Hoek, L.; Jones, I. M. Interaction of Severe Acute Respiratory Syndrome-Coronavirus and NL63 Coronavirus Spike Proteins with Angiotensin Converting Enzyme-2. *J. Gen. Virol.* **2008**, *89*, 2741.

(18) Lin, H. X.; Feng, Y.; Tu, X.; Zhao, X.; Hsieh, C. H.; Griffin, L.; Junop, M.; Zhang, C. Characterization of the Spike Protein of Human Coronavirus NL63 in Receptor Binding and Pseudotype Virus Entry. *Virus Res.* **2011**, *160*, 283−293.
(19) Walls, A. C.; Park, Y. J.; Tortorici, M. A.; Wall, A.; McGuire, A. T.; Veesler, D. Structure, Function, and Antigenicity of the SARS-CoV-2 Spike Glycoprotein. *Cell* **2020**, *181*, 281−292.
(20) Sternberg, A.; Naujokat, C. Structural Features of Coronavirus SARS-CoV-2 Spike Protein: Targets for Vaccination. *Life Sci.* **2020**, *257*, 118056.
(21) Li, F.; Li, W.; Farzan, M.; Harrison, S. C. Structure of SARS Coronavirus Spike Receptor-Binding Domain Complexed with Receptor. *Science* **2005**, *309*, 1864−1868.
(22) Lan, J.; Ge, J.; Yu, J.; Shan, S.; Zhou, H.; Fan, S.; Zhang, Q.; Shi, X.; Wang, Q.; Zhang, L.; Wang, X. Structure of the SARS-CoV-2 Spike Receptor-Binding Domain Bound to the ACE2 Receptor. *Nature* **2020**, *581*, 215−220.
(23) Wu, K.; Li, W.; Peng, G.; Li, F. Crystal Structure of NL63 Respiratory Coronavirus Receptor-Binding Domain Complexed with Its Human Receptor. *Proc. Natl. Acad. Sci. U.S.A.* **2009**, *106*, 19970−19974.
(24) Søndergaard, C. R.; Olsson, M. H. M.; Rostkowski, M.; Jensen, J. H. Improved Treatment of Ligands and Coupling Effects in Empirical Calculation and Rationalization of pK_a Values. *J. Chem. Theory Comput.* **2011**, *7*, 2284−2295.
(25) Momany, F. A.; Rone, R. Validation of the General Purpose QUANTA® 3.2/CHARMm® Force Field. *J. Comput. Chem.* **1992**, *13*, 888−900.
(26) Lima Neto, J. X.; Bezerra, K. S.; Barbosa, E. D.; Oliveira, J. I.; Manzoni, V.; Soares-Rachetti, V. P.; Albuquerque, E. L.; Fulco, U. L. Exploring the Binding Mechanism of GABAB Receptor Agonists and Antagonists Through In Silico Simulations. *J. Chem. Inf. Model.* **2020**, *60*, 1005−1018.
(27) Frisch, M. J.; Trucks, G. W.; Schlegel, H. B.; Scuseria, G. E.; Robb, M. A.; Cheeseman, J. R.; Scalmani, G.; Barone, V.; Mennucci, B.; Petersson, G. A.; Nakatsuji, H.; Caricato, M.; Li, X.; Hratchian, H. P.; Izmaylov, A. F.; Bloino, J.; Zheng, G.; Sonnenberg, J. L.; Hada, M.; Ehara, M.; Toyota, K.; Fukuda, R.; Hasegawa, J.; Ishida, M.; Nakajima, T.; Honda, Y.; Kitao, O.; Nakai, H.; Vreven, T.; Montgomery, J. A., Jr.; Peralta, P. E.; Ogliaro, F.; Bearpark, M.; Heyd, J. J.; Brothers, E.; Kudin, K. N.; Staroverov, V. N.; Kobayashi, R.; Normand, J.; Raghavachari, K.; Rendell, A.; Burant, J. C.; Iyengar, S. S.; Tomasi, J.; Cossi, M.; Rega, N.; Millam, N. J.; Klene, M.; Knox, J. E.; Cross, J. B.; Bakken, V.; Adamo, C.; Jaramillo, J.; Gomperts, R.; Stratmann, R. E.; Yazyev, O.; Austin, A. J.; Cammi, R.; Pomelli, C.; Ochterski, J. W.; Martin, R. L.; Morokuma, K.; Zakrzewski, V. G.; Voth, G. A.; Salvador, P.; Dannenberg, J. J.; Dapprich, S.; Daniels, A. D.; Farkas, Ö.; Ortiz, J. V.; Cioslowski, J.; Fox, D. J. *Gaussian 09*, Gaussian, Inc.: Wallingford, CT, 2009.
(28) Grimme, S. Semiempirical GGA-Type Density Functional Constructed with a Long-Range Dispersion Correction. *J. Comput. Chem.* **2006**, *27*, 1787−1799.
(29) Zhang, Z.-Y.; Liu, J.-M. Quantum mechanical calculation of nanomaterial-ligand interaction energies by molecular fractionation with conjugated caps method. *Sci. Rep.* **2017**, *7*, 1−16.
(30) Li, A.; Muddana, H. S.; Gilson, M. K. Quantum mechanical calculation of noncovalent interactions: a large-scale evaluation of PMx, DFT, and SAPT approaches. *J. Chem. Theory Comput.* **2014**, *10*, 1563−1575.
(31) Barone, V.; Cossi, M. Quantum Calculation of Molecular Energies and Energy Gradients in Solution by a Conductor Solvent Model. *J. Phys. Chem. A* **1998**, *102*, 1995−2001.
(32) Cossi, M.; Rega, N.; Scalmani, G.; Barone, V. Energies, Structures, and Electronic Properties of Molecules in Solution with the C-PCM Solvation Model. *J. Comput. Chem.* **2003**, *24*, 669−681.
(33) Tavares, A. B. M.; Lima Neto, J. X.; Fulco, U. L.; Albuquerque, E. L. Inhibition of the Checkpoint Protein PD-1 by the Therapeutic Antibody Pembrolizumab Outlined by Quantum Chemistry. *Sci. Rep.* **2018**, *8*, 1−13.
(34) Vicatos, S.; Roca, M.; Warshel, A. Effective Approach for Calculations of Absolute Stability of Proteins Using Focused Dielectric Constants. *Proteins* **2009**, *77*, 670−684.
(35) Morais, P. A.; Maia, F. F.; Solis-Calero, C.; Caetano, E. W. S.; Freire, V. N.; Carvalho, H. F. The Urokinase Plasminogen Activator Binding to Its Receptor: A Quantum Biochemistry Description within an in/Homogeneous Dielectric Function Framework with Application to uPA−uPAR Peptide Inhibitors. *Phys. Chem. Chem. Phys.* **2020**, *22*, 3570−3583.
(36) Zhang, D. W.; Zhang, J. Molecular Fractionation with Conjugate Caps for Full Quantum Mechanical Calculation of Protein−Molecule Interaction Energy. *J. Chem. Phys.* **2003**, *119*, 3599−3605.
(37) da Costa, R. F.; Freire, V. N.; Bezerra, E. M.; Cavada, B. S.; Caetano, E. W.; de Lima Filho, J. L.; Albuquerque, E. L. Explaining Statin Inhibition Effectiveness of HMG-CoA Reductase by Quantum Biochemistry Computations. *Phys. Chem. Chem. Phys.* **2012**, *14*, 1389−1398.
(38) Rodrigues, C. R. F.; Oliveira, J. I. N.; Fulco, U. L.; Albuquerque, E. L.; Moura, R. M.; Caetano, E. W. S.; Freire, V. N. Quantum Biochemistry Study of the T3−785 Tropocollagen Triple-Helical Structure. *Chem. Phys. Lett.* **2013**, *559*, 88−93.
(39) Lima Neto, J. X.; Soares-Rachetti, V. P.; Albuquerque, E. L.; Manzoni, V.; Fulco, U. L. Outlining Migrainous through Dihydroergotamine−Serotonin Receptor Interactions Using Quantum Biochemistry. *New J. Chem.* **2018**, *42*, 2401−2412.
(40) Pereira, A.; Bezerra, K.; Santos, J.; Oliveira, J. I.; Freire, V.; Fulco, U. L. Silico Approach of Modified Melanoma Peptides and Their Immunotherapeutic Potential. *Phys. Chem. Chem. Phys.* **2021**, *23*, 2836−2845.
(41) Bezerra, K. S.; Oliveira, J. I. N.; Lima Neto, J. X.; Albuquerque, E. L.; Caetano, E. W.; Freire, V. N.; Fulco, U. L. Quantum Binding Energy Features of the T3−785 Collagen-Like Triple-Helical Peptide. *RSC Adv.* **2017**, *7*, 2817−2828.
(42) Wang, Y.; Liu, J.; Li, J.; He, X. Fragment-Based Quantum Mechanical Calculation of Protein−Protein Binding Affinities. *J. Comput. Chem.* **2018**, *39*, 1617−1628.
(43) Albuquerque, E. L.; Fulco, U. L.; Caetano, E. W.; Freire, V. N. *Quantum Chemistry Simulation of Biological Molecules*; Cambridge University Press, 2021.
(44) He, X.; Zhu, T.; Wang, X.; Liu, J.; Zhang, J. Z. H. Fragment Quantum Mechanical Calculation of Proteins and Its Applications. *Acc. Chem. Res.* **2014**, *47*, 2748−2757.
(45) *Discovery Studio Visualizer*; Biovia, Dassault Systèmes, San Diego, CA, USA, 2021.
(46) Silva, S. R. B.; de Lima Neto, J. X.; Fuzo, C. A.; Fulco, U. L.; Vieira, D. S. A Quantum Biochemistry Investigation of the Protein−Protein Interactions for the Description of Allosteric Modulation on Biomass-Degrading Chimera. *Phys. Chem. Chem. Phys.* **2020**, *22*, 25936−25948.
(47) Wu, K.; Chen, L.; Peng, G.; Zhou, W.; Pennell, C. A.; Mansky, L. M.; Geraghty, R. J.; Li, F. A Virus-Binding Hot Spot on Human Angiotensin-Converting Enzyme 2 Is Critical for Binding of Two Different Coronaviruses. *J. Virol.* **2011**, *85*, 5331−5337.
(48) Rawat, P.; Jemimah, S.; Ponnuswamy, P.; Gromiha, M. M. Why are ACE2 Binding Coronavirus Strains SARS-CoV/SARS-CoV-2 Wild and NL63 Mild? *Proteins* **2021**, *89*, 389−398.
(49) Han, Y.; Král, P. Computational Design of ACE2-Based Peptide Inhibitors of SARS-CoV-2. *ACS Nano* **2020**, *14*, 5143−5147.
(50) Roy, S.; Jaiswar, A.; Sarkar, R. Dynamic Asymmetry Exposes 2019-nCoV Prefusion Spike. *J. Phys. Chem. Lett.* **2020**, *11*, 7021−7027.
(51) Spinello, A.; Saltalamacchia, A.; Magistrato, A. Is the Rigidity of SARS-CoV-2 Spike Receptor-Binding Motif the Hallmark for Its Enhanced Infectivity? Insights from All-Atom Simulations. *J. Phys. Chem. Lett.* **2020**, *11*, 4785−4790.
(52) Watanabe, K.; Watanabe, C.; Honma, T.; Tian, Y.-S.; Kawashima, Y.; Kawashita, N.; Takagi, T.; Fukuzawa, K. Intermolecular Interaction Analyses on SARS-CoV-2 Spike Protein Receptor

https://doi.org/10.1021/acs.jcim.1c01544
J. Chem. Inf. Model. XXXX, XXX, XXX−XXX

Binding Domain and Human Angiotensin-Converting Enzyme 2 Receptor-Blocking Antibody/Peptide Using Fragment Molecular Orbital Calculation. *J. Phys. Chem. Lett.* **2021**, *12*, 4059−4066.
(53) Adhikari, P.; Li, N.; Shin, M.; Steinmetz, N. F.; Twarock, R.; Podgornik, R.; Ching, W.-Y. Intra−and Intermolecular Atomic-Scale Interactions in the Receptor Binding Domain of SARS-CoV-2 Spike Protein: Implication for ACE2 Receptor Binding. *Phys. Chem. Chem. Phys.* **2020**, *22*, 18272−18283.
(54) Brielle, E. S.; Schneidman-Duhovny, D.; Linial, M. The SARS-CoV-2 Exerts a Distinctive Strategy for Interacting with the ACE2 Human Receptor. *Viruses* **2020**, *12*, 497.
(55) Jafary, F.; Jafari, S.; Ganjalikhany, M. R. In Silico Investigation of Critical Binding Pattern in SARS-CoV-2 Spike Protein with Angiotensin-Converting Enzyme 2. *Sci. Rep.* **2021**, *11*, 1−13.
(56) Lim, H.; Baek, A.; Kim, J.; Kim, M. S.; Liu, J.; Nam, K.-Y.; Yoon, J.; No, K. T. Hot Spot Profiles of SARS-CoV-2 and Human ACE2 Receptor Protein Protein Interaction Obtained by Density Functional Tight Binding Fragment Molecular Orbital Method. *Sci. Rep.* **2020**, *10*, 1−8.
(57) Andrade, J.; Gonçalves, P. F. B.; Netz, P. A. Why Does the Novel Coronavirus Spike Protein Interact So Strongly with the Human ACE2? A Thermodynamic Answer. *ChemBioChem.* **2021**, *22*, 865−875.
(58) Othman, H.; Bouslama, Z.; Brandenburg, J.-T.; Da Rocha, J.; Hamdi, Y.; Ghedira, K.; Srairi-Abid, N.; Hazelhurst, S. Interaction of the Spike Protein RBD from SARS-CoV-2 with ACE2: Similarity with SARS-CoV, Hot-Spot Analysis and Effect of the Receptor Polymorphism. *Biochem. Biophys. Res. Commun.* **2020**, *527*, 702−708.
(59) Chowdhury, R.; Boorla, V. S.; Maranas, C. D. Computational Biophysical Characterization of the SARS-CoV-2 Spike Protein Binding with the ACE2 Receptor and Implications for Infectivity. *Comput. Struct. Biotechnol. J.* **2020**, *18*, 2573−2582.
(60) Rodriguez, J. H.; Gupta, A. Contact Residue Contributions to Interaction Energies between SARS-CoV-1 Spike Proteins and Human ACE2 Receptors. *Sci. Rep.* **2021**, *11*, 1−12.
(61) Guruprasad, L. Human Coronavirus Spike Protein-Host Receptor Recognition. *Prog. Biophys. Mol. Biol.* **2021**, *161*, 39−53.
(62) Amin, M.; Sorour, M. K.; Kasry, A. Comparing the Binding Interactions in the Receptor Binding Domains of SARS-CoV-2 and SARS-CoV. *J. Phys. Chem. Lett.* **2020**, *11*, 4897−4900.
(63) Yan, R.; Zhang, Y.; Li, Y.; Xia, L.; Guo, Y.; Zhou, Q. Structural Basis for the Recognition of SARS-CoV-2 by Full-Length Human ACE2. *Science* **2020**, *367*, 1444−1448.
(64) Hwang, W. C.; Lin, Y.; Santelli, E.; Sui, J.; Jaroszewski, L.; Stec, B.; Farzan, M.; Marasco, W. A.; Liddington, R. C. Structural Basis of Neutralization by a Human Anti-severe Acute Respiratory Syndrome Spike Protein Antibody, 80R. *J. Biol. Chem.* **2006**, *281*, 34610−34616.
(65) Li, W.; Zhang, C.; Sui, J.; Kuhn, J. H.; Moore, M. J.; Luo, S.; Wong, S. K.; Huang, I. C.; Xu, K.; Vasilieva, N.; Murakami, A.; He, Y.; Marasco, W. A.; Guan, Y.; Choe, H.; Farzan, M. Receptor and Viral Determinants of SARS-Coronavirus Adaptation to Human ACE2. *EMBO J.* **2005**, *24*, 1634−1643.
(66) Watanabe, K.; Watanabe, C.; Honma, T.; Tian, Y.-S.; Kawashima, Y.; Kawashita, N.; Fukuzawa, K.; Takagi, T. Computational Ab Initio Interaction Analyses between Neutralizing Antibody and SARS-CoV-2 Variant Spike Proteins Using the Fragment Molecular Orbital Method. *Bull. Chem. Soc. Jpn.* **2021**, *94*, 1794−1798.
(67) Watanabe, C.; Okiyama, Y.; Tanaka, S.; Fukuzawa, K.; Honma, T. Molecular Recognition of SARS-CoV-2 Spike Glycoprotein: Quantum Chemical Hot Spot and Epitope Analyses. *Chem. Sci.* **2021**, *12*, 4722−4739.
(68) Akisawa, K.; Hatada, R.; Okuwaki, K.; Mochizuki, Y.; Fukuzawa, K.; Komeiji, Y.; Tanaka, S. Interaction Analyses of SARS-CoV-2 Spike Protein Based on Fragment Molecular Orbital Calculations. *RSC Adv.* **2021**, *11*, 3272−3279.
(69) Akisawa, K.; Hatada, R.; Okuwaki, K.; Kitahara, S.; Tachino, Y.; Mochizuki, Y.; Komeiji, Y.; Tanaka, S. Fragment Molecular Orbital Based Interaction Analyses on Complexes between SARS-CoV-2 RBD Variants and ACE2. *Jpn. J. Appl. Phys.* **2021**, *60*, 090901.
(70) Ishikawa, T.; Ozono, H.; Akisawa, K.; Hatada, R.; Okuwaki, K.; Mochizuki, Y. Interaction Analysis on the SARS-CoV-2 Spike Protein Receptor Binding Domain Using Visualization of the Interfacial Electrostatic Complementarity. *J. Phys. Chem. Lett.* **2021**, *12*, 11267−11272.
(71) Yi, C.; Sun, X.; Ye, J.; Ding, L.; Liu, M.; Yang, Z.; Lu, X.; Zhang, Y.; Ma, L.; Gu, W.; Qu, A.; Xu, J.; Shi, Z.; Ling, Z.; Sun, B. Key Residues of the Receptor Binding Motif in the Spike Protein of SARS-CoV-2 That Interact with ACE2 and Neutralizing Antibodies. *Cell. Mol. Immunol.* **2020**, *17*, 621−630.
(72) Zou, J.; Yin, J.; Fang, L.; Yang, M.; Wang, T.; Wu, W.; Bellucci, M. A.; Zhang, P. Computational Prediction of Mutational Effects on SARS-CoV-2 Binding by Relative Free Energy Calculations. *J. Chem. Inf. Model.* **2020**, *60*, 5794−5802.
(73) Harvey, W. T.; Carabelli, A. M.; Jackson, B.; Gupta, R. K.; Thomson, E. C.; Harrison, E. M.; Ludden, C.; Reeve, R.; Rambaut, A.; Peacock, S. J.; Robertson, D. L. SARS-CoV-2 Variants, Spike Mutations and Immune Escape. *Nat. Rev. Microbiol.* **2021**, *19*, 409−424.
(74) Taka, E.; Yilmaz, S. Z.; Golcuk, M.; Kilinc, C.; Aktas, U.; Yildiz, A.; Gur, M. Critical Interactions between the SARS-CoV-2 Spike Glycoprotein and the Human ACE2 Receptor. *J. Phys. Chem. B* **2021**, *125*, 5537−5548.
(75) Laffeber, C.; de Koning, K.; Kanaar, R.; Lebbink, J. H. Experimental Evidence for Enhanced Receptor Binding by Rapidly Spreading SARS-CoV-2 Variants. *J. Mol. Biol.* **2021**, *433*, 167058.
(76) Jawad, B.; Adhikari, P.; Podgornik, R.; Ching, W. Y. Key Interacting Residues between RBD of SARS-CoV-2 and ACE2 Receptor: Combination of Molecular Dynamic Simulation and Density Functional Calculation. *J. Chem. Inf. Model.* **2021**, *61*, 4425−4441.
(77) Yang, Y.; Zhang, Y.; Qu, Y.; Zhang, C.; Liu, X. W.; Zhao, M.; Mu, Y.; Li, W. Key Residues of the Receptor Binding Domain in the Spike Protein of SARS-CoV-2 Mediating the Interactions with ACE2: A Molecular Dynamics Study. *Nanoscale* **2021**, *13*, 9364−9370.
(78) Lin, H. X.; Feng, Y.; Wong, G.; Wang, L.; Li, B.; Zhao, X.; Li, Y.; Smaill, F.; Zhang, C. Identification of Residues in the Receptor-Binding Domain (RBD) of the Spike Protein of Human Coronavirus NL63 That Are Critical for the RBD−ACE2 Receptor Interaction. *J. Gen. Virol.* **2008**, *89*, 1015−1024.

https://doi.org/10.1021/acs.jcim.1c01544
J. Chem. Inf. Model. XXXX, XXX, XXX−XXX